

Cite this: *J. Mater. Chem. C*, 2016,
4, 596

Solid solution between lithium-rich yttrium and europium molybdate as new efficient red-emitting phosphors†

C. Litterscheid,^a S. Krüger,^b M. Euler,^c A. Dreizler,^c C. Wickleder*^b and B. Albert*^a

$\text{Li}_{3.5}\text{Y}_{1.5}(\text{MoO}_4)_4$ was synthesized in the form of phase-pure crystals. It forms a solid solution with $\text{Li}_{3.5}\text{Eu}_{1.5}(\text{MoO}_4)_4$. Single crystals obtained from Li_2MoO_4 fluxes had edge lengths of up to 0.5 mm. The crystal structures of $\text{Li}_{3.5}(\text{Y}_{1-x}\text{Eu}_x)_{1.5}(\text{MoO}_4)_4$ ($x = 0, 0.1, 0.25, 0.5, 0.75$ and 1) were determined in the triclinic crystal system (e.g. $P\bar{1}$, no. 2, $Z = 1$; $\text{Li}_{3.5}\text{Y}_{1.5}(\text{MoO}_4)_4$: $a = 5.1875(2)$ Å, $b = 6.6380(2)$ Å, $c = 10.2731(4)$ Å, $\alpha = 100.082(3)^\circ$, $\beta = 100.257(2)^\circ$ and $\gamma = 111.943(2)^\circ$). All the compounds are isostructural and crystallize with a structure related to the scheelite-type structure with mixed occupancy of one cation position, while the two others are occupied by Li ions exclusively. Thermal analyses reveal stability in air up to 995 K for $\text{Li}_{3.5}\text{Y}_{1.5}(\text{MoO}_4)_4$; the decomposition temperature decreases with an increase in Eu-content. Spectroscopic properties (emission and excitation) were investigated in the context of the search for new thermographic phosphors. Excitation at 395 nm leads to strong red emission at 613 nm. Features of the emission spectra suggest the potential of $\text{Li}_{3.5}(\text{Y}_{1-x}\text{Eu}_x)_{1.5}(\text{MoO}_4)_4$ as red phosphor candidates for light emitting diodes. Their luminescence properties at high temperatures were also investigated.

Received 12th August 2015,
Accepted 7th December 2015

DOI: 10.1039/c5tc02515j

www.rsc.org/MaterialsC

1. Introduction

Currently, there is a drastic change in the illumination technology due to the substitution of incandescent and discharge lamps by energy saving light emitting diodes (LEDs). The general strategy is the combination of near UV emitting Ga/InN LEDs with red, green and blue emitting phosphors.¹ Numerous respective materials are

available, which emit in the high energy visible range, but still there is a demand for red emitting phosphors. Eu^{2+} doped nitrides are very promising candidates in this context but include some disadvantages. Eu^{3+} doped materials are well known alternatives due to the $4f^6 \rightarrow 4f^6$ emission located in the red region typical for Eu^{3+} ions. The narrow line emission of Eu^{3+} ions gives high colour quality devices, compared to the band emission of Eu^{2+} ions. A remarkable drawback is, however, that direct excitation into the $4f^6$ states leads to inefficient emission due to parity forbidden $f \leftrightarrow f$ transitions. A solution to this problem is the development of host lattices with complex anions, which include highly charged central atoms, e.g. tungstates and molybdates. In these cases, the charge transfer states of the complex anions are located at rather low energies, namely, in the near UV region and can thus be excited by Ga/InN LEDs. Intense Eu^{3+} red emission is achieved after energy transfer from CT to the $4f^6$ states. Moreover, these materials fulfil the requirements for luminescent materials such as high chemical and thermal stability and a suitable site for Eu^{3+} doping. Herein, we present a new material, $\text{Li}_{3.5}\text{Y}_{1.5}(\text{MoO}_4)_4:\text{Eu}^{3+}$, which shows a strong red narrow line emission.

Contrary to $\text{Li}_{3.5}\text{RE}_{1.5}(\text{MoO}_4)_4$, lithium rare earth metal molybdates of the general formula, $\text{LiRE}(\text{MoO}_4)_2$ (RE: La–Lu, Y), are well-known and crystallize in the tetragonal crystal system with a scheelite-type structure (Scheelite: CaWO_4). They are obtained from $\text{LiF}-\text{MoO}_3^2$ or $\text{Li}_2\text{MoO}_4^{3-6}$ fluxes and have been

^a Eduard-Zintl-Institut für Anorganische und Physikalische Chemie, Technische Universität Darmstadt, Alarich-Weiss-Straße 12, 64287 Darmstadt, Germany. E-mail: albert@ac.chemie.tu-darmstadt.de; Fax: +49-6151-16-6029; Tel: +49-6151-16-2392

^b Department Chemie-Biologie – Anorganische Chemie, Universität Siegen, Adolf-Reichwein-Straße 2, 57068 Siegen, Germany; E-mail: wickleder@chemie.uni-siegen.de; Fax: +49-271-740-2555; Tel: +49-271-740-4217

^c FG Reaktive Strömungen und Messtechnik, Maschinenbau/Center of Smart Interfaces, Technische Universität Darmstadt, Jovanka-Bontschits-Straße 2, 64287 Darmstadt, Germany

† Electronic supplementary information (ESI) available: Atomic coordinates and displacement parameters of $\text{Li}_{3.5}(\text{Y}_{1-x}\text{Eu}_x)_{1.5}(\text{MoO}_4)_4$ ($x = 0, 0.1, 0.25, 0.5, 0.75, 1$) (Tables S1a–S2f), selected interatomic distances and angles (Table S3a–f and Fig. S1–S5). Further details of the crystal structure investigation may be obtained from Fachinformationszentrum Karlsruhe, 76344 Eggenstein-Leopoldshafen, Germany [E-mail: crysdata@fiz-karlsruhe.de; Web: http://www.fiz-karlsruhe.de/request_for_deposited_data.html; Fax: (+49)7247-808-666] upon quoting the CSD numbers for $\text{Li}_{3.5}(\text{Y}_{1-x}\text{Eu}_x)_{1.5}(\text{MoO}_4)_4$ ($x = 0.00$: 427655; $x = 0.10$: 427656; $x = 0.25$: 427657; $x = 0.50$: 427658; $x = 0.75$: 427659; $x = 1.00$: 425893). See DOI: 10.1039/c5tc02515j



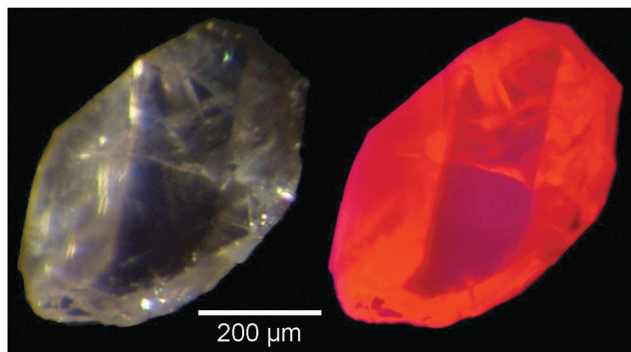


Fig. 1 Crystal of $\text{Li}_{3.5}\text{Eu}_{1.5}(\text{MoO}_4)_4$ under day light (left) and UV light (right).

investigated for many decades, mainly as host materials for optical materials. The luminescence properties of Eu^{3+} -doped molybdates $\text{LiRE}(\text{MoO}_4)_2:\text{Eu}$ (RE: La, Gd, Lu and Y),^{7–9} $\text{LiEu}(\text{Mo}_{1-x}\text{W}_x\text{O}_4)_2$ ¹⁰ and $\text{AY}_{1-x}\text{Eu}_x(\text{MoO}_4)_2$ (A: Li, Na, K)^{11–17} have been described in the literature.

When it comes to lithium rare earth metal molybdates of the general formula $\text{Li}_{3.5}\text{RE}_{1.5}(\text{MoO}_4)_4$, the crystal structures of only two representatives are known: $\text{Li}_{3.5}\text{Ho}_{1.5}(\text{MoO}_4)_4$ and $\text{Li}_{3.5}\text{Eu}_{1.5}(\text{MoO}_4)_4$.^{18,19} In addition, $\text{Li}_{3.5}\text{Y}_{1.5}(\text{MoO}_4)_4$ was found to crystallize from $\text{Li}_2(\text{MoO}_4)_2$ – $\text{LiY}(\text{MoO}_4)_2$ flux, but its structure has not been determined.²⁰ Its *d* values resemble that of a compound that was (wrongly) described to be a triclinic modification of $\text{LiY}(\text{MoO}_4)_2$.²¹

We will now describe for the first time the crystal structures of several red-emitting phosphors (Fig. 1) in the system $\text{Li}_{3.5}(\text{Y}_{1-x}\text{Eu}_x)_{1.5}(\text{MoO}_4)_4$ with $x = 0, 0.1, 0.25, 0.5, 0.75, 1$ and discuss their thermal stability and luminescence properties.

2. Experimental

Synthesis and crystallization

Lithium carbonate (Merck, PA), molybdenum trioxide (Alpha Aesar, 99.95%) and rare-earth oxides Y_2O_3 and Eu_2O_3 (Chempur, 99.99%) were used as starting materials. A mixture of Li_2CO_3 , RE_2O_3 ($1-x \text{ Y}_2\text{O}_3 + x \text{ Eu}_2\text{O}_3$) and MoO_3 powders in the molar ratio of $\text{Li}:\text{RE}:\text{Mo} = 36:2:21$ were first ground in an agate mortar and then transferred to a platinum crucible. The mixtures were heated in air from room temperature to 1373 K (100 K h^{-1}), maintained for six hours at the maximum temperature to homogenize the melt, then cooled to 1023 K at 100 K h^{-1} and to 773 K at 2 K h^{-1} . The melting point of pure Li_2MoO_4 is 978 K,²² but the solidification of the flux described here must take place below 957 K according to the decomposition temperatures observed for some of the products obtained (see below). Finally, the samples were quenched to room temperature. The Li_2MoO_4 -flux was dissolved in hot water.

Thermal analyses

Differential thermal analysis (DTA) and thermogravimetric analyses (TGA) were performed using an STA 409 EP instrument (Netzsch, Selb, Germany). The samples were heated from 293 K to 1073 K in air (5 K min^{-1}).

X-ray powder diffraction

Data were collected at room temperature using a powder diffractometer with transmission geometry (Stadi P, Stoe, Darmstadt, Germany, PSD detector, Ge monochromator, $\text{CuK}\alpha_1$; $\lambda = 1.54056 \text{ \AA}$, and flat plate sample holder). Phase analyses and the refinements of the lattice parameters were performed using the TOPAS program.²³

Single crystal diffractometry

Intensity data were measured on an image plate diffraction system (IPDS, Stoe, Darmstadt, Germany, $\text{MoK}\alpha$; $\lambda = 0.71073 \text{ \AA}$) at ambient temperatures. Numerical absorption corrections were applied using the X-RED and X-SHAPE software.²⁴ Structure refinements were performed using the SHELX-97²⁵ suite in the WinGX²⁶ framework. The normalized atomic coordinates of the isostructural compound $\text{Li}_{3.5}\text{Ho}_{1.5}(\text{MoO}_4)_4$ ¹⁸ were taken as starting values for all the least squares refinements.

Photoluminescence spectroscopy

Emission and excitation spectra of crystalline powders were acquired using a Fluorolog3 spectrofluorometer (Model F13-22, Horiba Jobin-Yvon, Bensheim, Germany) equipped with a 450 W xenon lamp, double Czerny–Turner monochromators, which allow a resolution down to 0.05 nm, and the photomultiplier detection equipment R928P with a photon counting system. A liquid Helium closed-cycle cryostat was used to perform measurements at 10 K. Emission spectra were corrected for the photomultiplier sensitivity and excitation spectra were corrected for the lamp intensity.

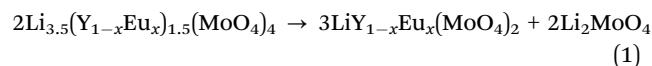
Quantum yield was measured using a Fluorolog3 spectrofluorometer with an additional Ulbricht sphere; reflection intensities were corrected.

3. Results and discussion

Samples of $\text{Li}_{3.5}(\text{Y}_{1-x}\text{Eu}_x)_{1.5}(\text{MoO}_4)_4$ with $x = 0, 0.1, 0.25, 0.5, 0.75$ and 1 were obtained from high-temperature reactions in Li_2MoO_4 fluxes as single crystals. X-ray powder diffraction patterns (Fig. 2) of the crushed products show that mostly single-phase $\text{Li}_{3.5}(\text{Y}_{1-x}\text{Eu}_x)_{1.5}(\text{MoO}_4)_4$ samples were obtained (except for 2% of the side product $\text{LiEu}(\text{MoO}_4)_2$ in one of the samples; its main reflection is marked with an asterisk).

Thermal analyses reveal that $\text{Li}_{3.5}(\text{Y}_{1-x}\text{Eu}_x)_{1.5}(\text{MoO}_4)_4$ are stable up to 995 K, which makes them suitable materials for light emitting diodes. The decomposition temperatures according to DTA depend remarkably on their composition (Fig. 3). For undoped $\text{Li}_{3.5}\text{Y}_{1.5}(\text{MoO}_4)_4$, a decomposition temperature of 995 K was measured, which is a bit lower than was reported earlier (1008 K).²⁰ With an increase in Eu^{3+} -substitution, the decomposition temperature decreases to 957 K for $\text{Li}_{3.5}(\text{Y}_{0.25}\text{Eu}_{0.75})_{1.5}(\text{MoO}_4)_4$. The decomposition of $\text{Li}_{3.5}\text{Eu}_{1.5}(\text{MoO}_4)_4$ takes place at 958 K and no weight changes were observed in the TGA traces.

X-ray powder diffraction investigations of the residues obtained after the DTA/TGA experiments showed that the samples decompose and form Li_2MoO_4 and $\text{LiY}_{1-x}\text{Eu}_x(\text{MoO}_4)_2$ (eqn (1)).



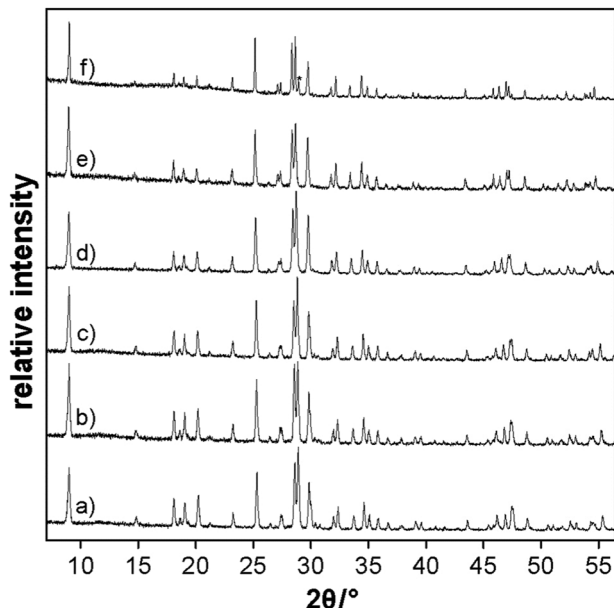


Fig. 2 X-ray powder diffraction patterns of $\text{Li}_{3.5}(\text{Y}_{1-x}\text{Eu}_x)_{1.5}(\text{MoO}_4)_4$ (a) $x = 0.00$, (b) $x = 0.10$, (c) $x = 0.25$, (d) $x = 0.50$, (e) $x = 0.75$ and (f) $x = 1.00$ (the asterisk marks the main reflection of $\text{LiEu}(\text{MoO}_4)_2$, see text).

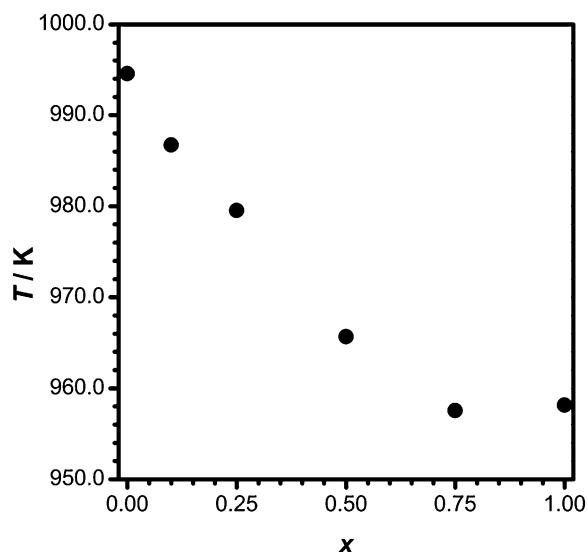


Fig. 3 Decomposition temperatures of $\text{Li}_{3.5}(\text{Y}_{1-x}\text{Eu}_x)_{1.5}(\text{MoO}_4)_4$.

The title compounds, $\text{Li}_{3.5}(\text{Y}_{1-x}\text{Eu}_x)_{1.5}(\text{MoO}_4)_4$, crystallize isostructurally to $\text{Li}_{3.5}\text{Ho}_{1.5}(\text{MoO}_4)_4$.¹⁸ Their lattice parameters change continuously with an increase in Eu^{3+} concentration (Table 1).

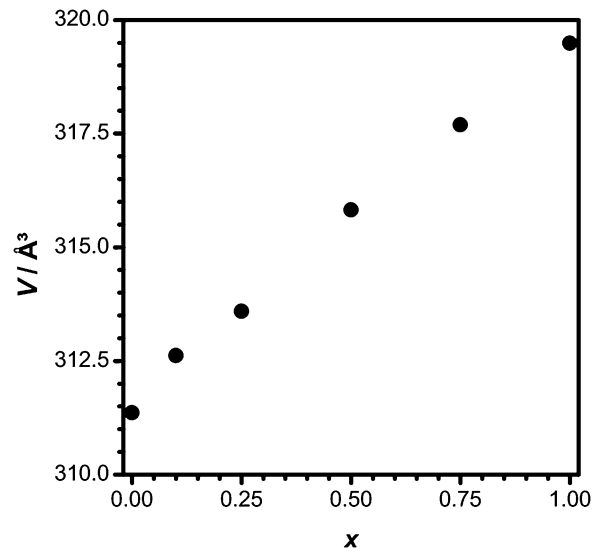


Fig. 4 V/x dependence of $\text{Li}_{3.5}(\text{Y}_{1-x}\text{Eu}_x)_{1.5}(\text{MoO}_4)_4$.

Fig. 4 demonstrates the linear increase of the unit cell volume with an increase in x . The pseudo-binary system $\text{Li}_{3.5}\text{Y}_{1.5}(\text{MoO}_4)_4$ – $\text{Li}_{3.5}\text{Eu}_{1.5}(\text{MoO}_4)_4$ thus forms a solid solution, and the lattice parameters follow Vegard's law. x values obtained from the powder data agree well with the expected Eu content according to the original sample weight.

The color of the crystals changes from colorless for the pure yttrium-compound to light pinkish for the pure europium-compound.

The crystal structures of $\text{Li}_{3.5}(\text{Y}_{1-x}\text{Eu}_x)_{1.5}(\text{MoO}_4)_4$ with $x = 0, 0.1, 0.25, 0.5, 0.75$ and 1.0 were refined based on single-crystal data (Table 2). They consist of layers of isolated $[\text{MoO}_4]$ tetrahedra and distorted $[\text{MO}_8]$ square antiprisms (M: 25% Li + 75% RE with RE = $\text{Y}_{1-x}\text{Eu}_x$) (Fig. 5). The arrangement of the $[\text{MO}_8]$ (RE1 and Li1 site) and $[\text{MoO}_4]$ polyhedra is similar to that in scheelite. The layers are perpendicular to (001). Additional Li atoms are placed on the Li2 and Li3 sites (Wyckoff position 1a) in between the layers. Li2 is coordinated by four oxygen atoms, which form a rectangle. The coordination sphere of the lithium ions on the Li3 site is that of a distorted octahedron of oxygen atoms. The ratio of Li1 and RE1 on the substitutionally disordered M1 site was found to be very close to 1:3 by refining the occupancies. In a later refinement cycle, these values were fixed to ensure charge balance. The positional and anisotropic displacement parameters of Li1 and RE1 atoms were constrained to be identical.²⁵ The final atomic coordinates and displacement parameters are reported in the supplementary

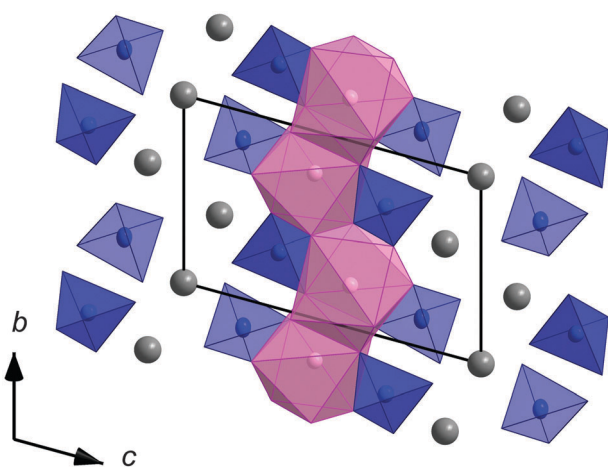
Table 1 Lattice parameters of $\text{Li}_{3.5}(\text{Y}_{1-x}\text{Eu}_x)_{1.5}(\text{MoO}_4)_4$ ($x = 0.00, 0.10, 0.25, 0.50, 0.75$ and 1.00) with a triclinic $\text{Li}_{3.5}\text{Ho}_{1.5}(\text{MoO}_4)_4$ structure

Formulae	x	$a/\text{Å}$	$b/\text{Å}$	$c/\text{Å}$	$\alpha/^\circ$	$\beta/^\circ$	$\gamma/^\circ$	$V/\text{Å}^3$
$\text{Li}_{3.5}\text{Y}_{1.5}(\text{MoO}_4)_4$	0.00	5.1875(2)	6.6380(2)	10.2731(4)	100.082(3)	100.257(2)	111.943(2)	311.36(2)
$\text{Li}_{3.5}\text{Y}_{1.35}\text{Eu}_{0.15}(\text{MoO}_4)_4$	0.10	5.1944(2)	6.6500(2)	10.2825(4)	100.086(3)	100.273(3)	111.931(2)	312.62(2)
$\text{Li}_{3.5}\text{Y}_{1.125}\text{Eu}_{0.375}(\text{MoO}_4)_4$	0.25	5.1993(2)	6.6615(2)	10.2876(4)	100.100(2)	100.300(2)	111.914(2)	313.59(2)
$\text{Li}_{3.5}\text{Y}_{0.75}\text{Eu}_{0.75}(\text{MoO}_4)_4$	0.50	5.2107(3)	6.6850(4)	10.3025(7)	100.106(4)	100.362(4)	111.879(4)	315.82(4)
$\text{Li}_{3.5}\text{Y}_{0.375}\text{Eu}_{1.125}(\text{MoO}_4)_4$	0.75	5.2198(2)	6.7057(3)	10.3141(4)	100.116(3)	100.396(3)	111.860(2)	317.69(2)
$\text{Li}_{3.5}\text{Eu}_{1.5}(\text{MoO}_4)_4$	1.00	5.2283(3)	6.7253(3)	10.3267(6)	100.116(4)	100.450(3)	111.840(3)	319.49(3)



Table 2 Crystallographic data, data collection and refinement of the crystal structures of $\text{Li}_{3.5}\text{Y}_{1-x}\text{Eu}_x\text{Li}_{1.5}(\text{MoO}_4)_4$ (x : 0.00, 0.10, 0.25, 0.50, 0.75 and 1.00)

Composition	$\text{Li}_{3.5}\text{Y}_{1.5}(\text{MoO}_4)_4$	$\text{Li}_{3.5}\text{Y}_{1.35}\text{Eu}_{0.15}(\text{MoO}_4)_4$	$\text{Li}_{3.5}\text{Y}_{1.125}\text{Eu}_{0.375}(\text{MoO}_4)_4$	$\text{Li}_{3.5}\text{Y}_{0.75}\text{Eu}_{0.75}(\text{MoO}_4)_4$	$\text{Li}_{3.5}\text{Y}_{0.375}\text{Eu}_{1.125}(\text{MoO}_4)_4$	$\text{Li}_{3.5}\text{Eu}_{1.5}(\text{MoO}_4)_4$
Molecular weight	797.42	806.87	821.06	844.7	868.35	891.99
Crystal system	Triclinic					
Space group	$P\bar{1}$ (no. 2)					
Lattice parameters	(From powder XRD data)					
$a/\text{\AA}$	5.1875(2)	5.1944(2)	5.1993(2)	5.2107(3)	5.2198(2)	5.2283(3)
$b/\text{\AA}$	6.6380(2)	6.6500(2)	6.6615(2)	6.6850(4)	6.7057(3)	6.7253(3)
$c/\text{\AA}$	10.2731(4)	10.2825(4)	10.2876(4)	10.3025(7)	10.3141(4)	10.3267(6)
$\alpha/^\circ$	100.082(3)	100.086(3)	100.100(2)	100.106(4)	100.116(3)	100.116(4)
$\beta/^\circ$	100.257(2)	100.273(3)	100.300(2)	100.362(4)	100.396(3)	100.450(3)
$\gamma/^\circ$	111.943(2)	111.931(2)	111.914(2)	111.879(4)	111.860(2)	111.840(3)
Unit cell volume/ \AA^3	311.36(2)	312.62(2)	313.59(2)	315.82(4)	317.69(2)	319.49(3)
Z	1					
Absorp. coeff./ mm^{-1}	10.92	10.93	10.99	11.03	11.09	11.15
Density (calculated)	4.253	4.286	4.348	4.441	4.539	4.636
Crystal colour	Colorless	Colorless	Colorless	Light pink	Light pink	Light pink
Crystal shape	Block	Block	Block	Block	Prism	Prism
Crystal size/ mm^3	0.40-0.35-0.30	0.27-0.22-0.15	0.47-0.34-0.21	0.42-0.32-0.22	0.29-0.22-0.09	0.35-0.20-0.07
$F(000)$	365	369	374	383	392	401
Temperature/K	293(2)	293(2)	293(2)	293(2)	293(2)	293(2)
Diffractometer	STOE IPDS 2, Mo-K α , $\lambda = 0.71073 \text{ \AA}$, graphite monochromator					
Absorption correction	Numerical ²⁴					
Theta range/ $^\circ$	2.09–30.35	2.09–30.44	2.09–30.39	3.41–30.27	2.08–30.28	2.08–30.40
Reflections collected	6526	6695	6726	6489	6524	6873
Independent reflections	1867	1893	1899	1868	1884	1931
	$(R_{\text{int}} = 0.0966)$	$(R_{\text{int}} = 0.0937)$	$(R_{\text{int}} = 0.1144)$	$(R_{\text{int}} = 0.1052)$	$(R_{\text{int}} = 0.0715)$	$(R_{\text{int}} = 0.0654)$
Independent reflections	1700	1636	1728	1534	1579	1566
$I > 2\sigma(I)$						
Index ranges	$-7 \leq h \leq 7$ $-9 \leq k \leq 9$ $-14 \leq l \leq 14$	$-6 \leq h \leq 7$ $-9 \leq k \leq 9$ $-14 \leq l \leq 14$	$-7 \leq h \leq 7$ $-9 \leq k \leq 9$ $-14 \leq l \leq 14$	$-7 \leq h \leq 7$ $-8 \leq k \leq 9$ $-14 \leq l \leq 14$	$-7 \leq h \leq 7$ $-9 \leq k \leq 9$ $-14 \leq l \leq 14$	$-7 \leq h \leq 7$ $-9 \leq k \leq 9$ $-14 \leq l \leq 14$
Parameters	106					
R indices/all data	$R_1 = 3.81\%$ $wR_2 = 9.35\%$	$R_1 = 4.29\%$ $wR_2 = 7.85\%$	$R_1 = 3.71\%$ $wR_2 = 8.72\%$	$R_1 = 4.30\%$ $wR_2 = 8.18\%$	$R_1 = 3.79\%$ $wR_2 = 7.25\%$	$R_1 = 3.70\%$ $wR_2 = 6.70\%$
R indices/ $I > 2\sigma(I)$	$R_1 = 3.41\%$ $wR_2 = 9.12\%$	$R_1 = 3.55\%$ $wR_2 = 7.59\%$	$R_1 = 3.38\%$ $wR_2 = 8.54\%$	$R_1 = 3.44\%$ $wR_2 = 7.88\%$	$R_1 = 3.06\%$ $wR_2 = 7.02\%$	$R_1 = 2.91\%$ $wR_2 = 6.50\%$
Goodness-of-fit on F^2	1.118					
Weighting scheme	$A = 0.0458$; $B = 0.2597$	$A = 0.0272$; $B = 0.5208$	$A = 0.0264$; $B = 0.4439$	$A = 0.0301$; $B = 0$	$A = 0.0263$; $B = 0.7076$	$A = 0.0330$; $B = 0$
Largest diff. peak and hole/ $e \text{ \AA}^{-3}$	–1.354	–1.299	–1.417	–1.391	–1.801	–2.105

Fig. 5 Crystal structure of $\text{Li}_{3.5}(\text{Y}_{1-x}\text{Eu}_x)_{1.5}(\text{MoO}_4)_4$ (blue: $[\text{MoO}_4]$ tetrahedra, pink: $[\text{MO}_8]$ polyhedra (M: 75% RE + 25% Li; RE: $\text{Y}_{1-x}\text{Eu}_x$) and grey: Li).

material (Tables S1a–S2f, ESI[†]), as well as selected interatomic distances and angles (Table S3a–f and Fig. S1–S5, ESI[†]).

All the samples of the solid solution show bright red emission, which is typical for Eu^{3+} phosphors. Luminescence measurements were performed on the unsubstituted material ($x = 1$) and on that with 10% doping concentration ($x = 0.1$). The room temperature emission and excitation spectra of the latter are shown in Fig. 6, while the emission and excitation spectra of both compounds at 10 K are depicted in Fig. 7 and 9, respectively. An enlargement of the emission spectrum at 10 K of $\text{Li}_{3.5}(\text{Y}_{0.9}\text{Eu}_{0.1})_{1.5}(\text{MoO}_4)_4$ is shown in Fig. 8.

The shape of the emission spectra at 10 K (Fig. 7) is remarkable because only the $^5\text{D}_0 \rightarrow ^7\text{F}_2$ transition has a considerable contribution, while $^5\text{D}_0 \rightarrow ^7\text{F}_{1,3,4}$ are rather weak and $^5\text{D}_0 \rightarrow ^7\text{F}_0$ is only visible with extremely low intensity (Fig. 8). This feature can be explained due the low site symmetry occupied by the Eu ions (point group C_i). In general, $^5\text{D}_0 \rightarrow ^7\text{F}_0$ are observed only for C_{nv} , C_n , or C_s symmetry, because this transition is strictly forbidden according to the Judd-Ofelt theory and only becomes partly allowed due to J-mixing.²⁶ In the present case, this observation might be explained by mixing of charge-transfer states into the wave functions of the $4f^6$ configuration.²⁷



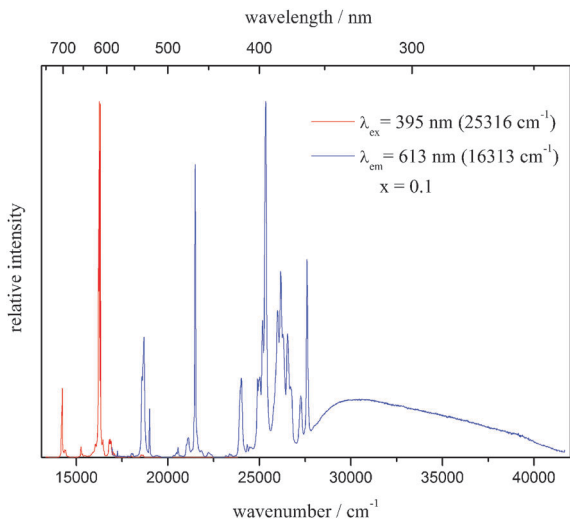


Fig. 6 Emission (left, red line) and excitation (right, blue line) of $\text{Li}_{3.5}(\text{Y}_{0.9}\text{Eu}_{0.1})_{1.5}(\text{MoO}_4)_4$ at room temperature.

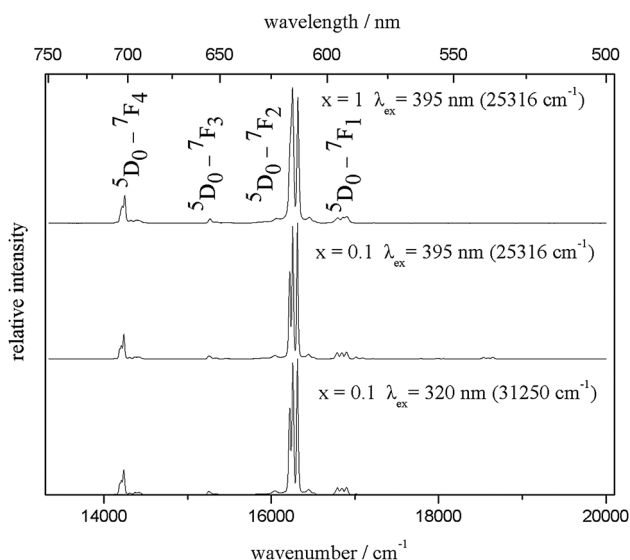


Fig. 7 Emission spectra of $\text{Li}_{3.5}(\text{Y}_{1-x}\text{Eu}_{0.1})_{1.5}(\text{MoO}_4)_4$ for $x = 1$ (top) and $x = 0.1$ (middle and bottom) measured at 10 K.

While in general, ${}^5\text{D}_0 \rightarrow {}^7\text{F}_1$ can be taken to be constant in intensity, the so called hypersensitive transition ${}^5\text{D}_0 \rightarrow {}^7\text{F}_2$ is mainly influenced by the environment. The ratio $I({}^5\text{D}_0 \rightarrow {}^7\text{F}_2)/I({}^5\text{D}_0 \rightarrow {}^7\text{F}_1)$ can be used to determine the degree of the asymmetry of the Eu site.²⁸ In the present case, this ratio was determined to be 11.3 for $\text{Li}_{3.5}\text{Eu}_{1.5}(\text{MoO}_4)_4$ and 12.2 for $\text{Li}_{3.5}(\text{Y}_{0.9}\text{Eu}_{0.1})_{1.5}(\text{MoO}_4)_4$. This high ratio can be explained by the low Eu site symmetry. It should be mentioned that the high intensity of ${}^5\text{D}_0 \rightarrow {}^7\text{F}_2$ relative to the other transitions depicts the excellent color quality of these materials. As it is obvious from Fig. 8, ${}^5\text{D}_0 \rightarrow {}^7\text{F}_1$ splits into three Stark levels, which led to the conclusion that the Eu ions occupy only one site, as described above. However, a small shoulder can be observed at about 598 nm. Therefore, it cannot be excluded that an extremely small amount of Eu^{3+} ions are also located at another site.

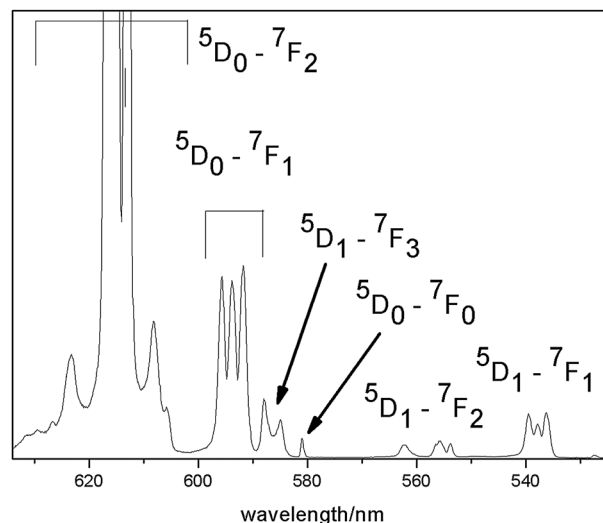


Fig. 8 Enlargement of the emission spectrum of $\text{Li}_{3.5}(\text{Y}_{0.9}\text{Eu}_{0.1})_{1.5}(\text{MoO}_4)_4$ at 10 K, $\lambda_{\text{ex}} = 395$ nm.

Moreover, some very weak emission transitions starting from the ${}^5\text{D}_1$ state could be observed even at 10 K (Fig. 8).

The low temperature excitation spectra (Fig. 9) consist of two different features. At energies lower than approximately $27\,500\text{ cm}^{-1}$, $4f^6 \rightarrow 4f^6$ line transitions are observed, which can be assigned to ${}^7\text{F}_0 \rightarrow {}^5\text{D}_1$ at 525.8 nm, ${}^7\text{F}_0 \rightarrow {}^5\text{D}_2$ at 465.2 nm and ${}^7\text{F}_0 \rightarrow {}^5\text{L}_6$ at 395.2 nm. The second feature is a broad band starting at approximately $28\,290\text{ cm}^{-1}$ (354 nm), which can be assigned to the charge-transfer excitation $\text{O}^{2-} \rightarrow \text{Mo}^{6+}$. After excitation into this CT state, no CT emission was observed, but only Eu^{3+} emission, which is identical to that detected after direct Eu excitation (Fig. 7, middle and bottom). This observation proves the high efficiency of the energy transfer process $\text{CT} \rightarrow \text{Eu}^{3+}$. The ratios of the integrated excitation intensities detecting Eu emission $I(\text{CT})/I(\text{Eu})$ are determined to be 1.23 for $x = 1$ and 5.48 for $x = 0.1$. The reason for this observation may

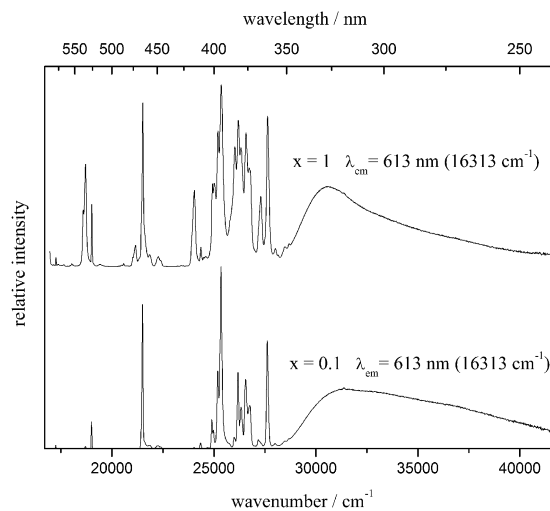


Fig. 9 Excitation spectra of $\text{Li}_{3.5}(\text{Y}_{1-x}\text{Eu}_{0.1})_{1.5}(\text{MoO}_4)_4$ for $x = 1$ (top) and $x = 0.1$ (bottom) at 10 K, $\lambda_{\text{em}} = 613$ nm.



not be the more intense energy transfer efficiency for the doped material, but the higher excitation probability of the CT transitions compared to Eu excitation due to the lower Eu concentration.

Quantum yield measurements of direct Eu excitation of the 10% doped material gave the remarkable value of 44%, and this may be explained by the low vibrational quenching processes in these compounds. The quantum yield of Eu emission after CT excitation is, however, decreased to 22%. Obviously, there are some other pathways to quench the excitation energy.

For applications of phosphors, it is important to investigate their thermal stability and the change in their luminescence properties at elevated temperatures because of the working temperatures of LEDs at 150–200 °C.²⁹ Therefore, the optical behavior at temperatures up to 375 °C was investigated. Fig. 10 depicts the temperature-dependent emission spectra. The emission intensity at 100 °C is approximately 70% of that at room temperature, while it drops to approximately 10% at 375 °C.

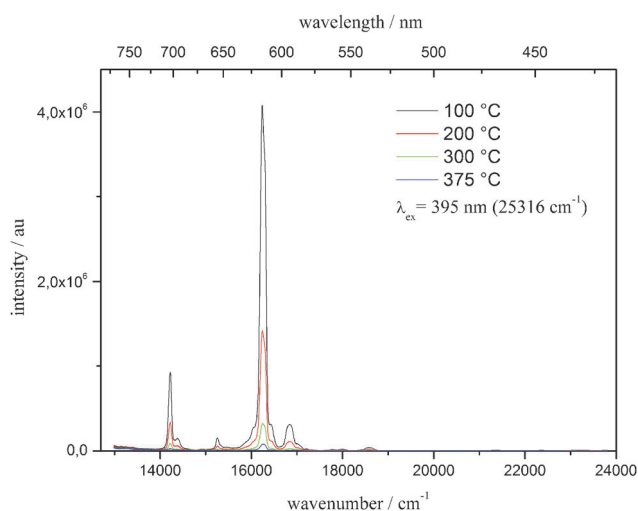


Fig. 10 Temperature-dependent emission spectra of $\text{Li}_{3.5}(\text{Y}_{0.9}\text{Eu}_{0.1})_{1.5}(\text{MoO}_4)_4$ between 100 and 375 °C, $\lambda_{\text{ex}} = 395$ nm.

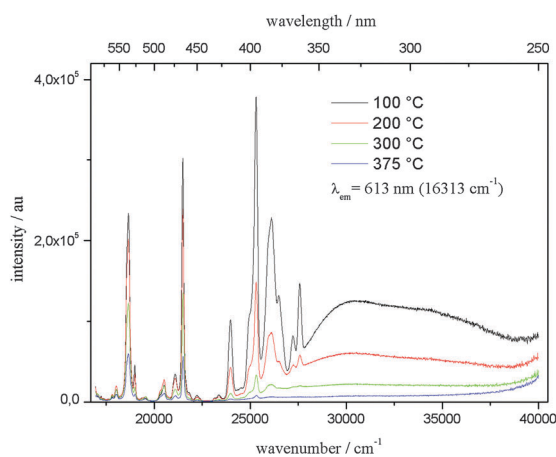


Fig. 11 Temperature-dependent excitation spectra of $\text{Li}_{3.5}(\text{Y}_{0.9}\text{Eu}_{0.1})_{1.5}(\text{MoO}_4)_4$ between 100 and 375 °C, $\lambda_{\text{em}} = 613$ nm.

The high-temperature excitation spectra are shown in Fig. 11. While the intensities of the 4f–4f excitation bands at high temperatures are, again, lowered to a rather large extent (at 375 °C to about 25% compared to that at room temperature), it is remarkable that the CT excitation band is nearly completely quenched at 375 °C. Obviously, the amount of vibrational radiationless relaxation is more efficient for the latter than for the 4f–4f excitation. This can be explained by the large increase in the Eu–O distances of the CT state compared to that of the ground state, which probably leads to coupling between the vibrational states of the excited and the ground state, which is not the case for the excited 4f states with comparable inter-nuclear distances of excited and ground states.

4. Conclusions

Crystals of the red-emitting phosphor $\text{Li}_{3.5}(\text{Y}_{1-x}\text{Eu}_x)_{1.5}(\text{MoO}_4)_4$ with $x = 0, 0.1, 0.25, 0.5, 0.75$ and 1 have been successfully synthesized *via* flux synthesis. Solid solutions in the pseudo-binary system of Y- and the Eu-compounds were observed and investigated for the first time. The crystal structures of $\text{Li}_{3.5}(\text{Y}_{1-x}\text{Eu}_x)_{1.5}(\text{MoO}_4)_4$ were determined. The fact that CT excitation followed by efficient energy transfer yielded intense red Eu^{3+} emission and also high color quality due to the large intensity of ${}^5\text{D}_0 \rightarrow {}^7\text{F}_2$ transitions with respect to the other intensities shows the qualification of these materials for future light-emitting diodes.

Acknowledgements

Financial support of the Deutsche Forschungsgemeinschaft (AL536/14-1, DR374/16-1) and the Darmstadt Graduate School of Excellence Energy Science and Engineering is gratefully acknowledged. We would like to thank Dipl.-Ing. Dennis Henge for DTA/TGA measurements.

Notes and references

- P. Pust, P. J. Schmidt and W. Schnick, *Nat. Mater.*, 2015, **14**, 454–458.
- U. Kolitsch, *Z. Kristallogr.*, 2001, **216**, 449–454.
- Y. W. Wei, Y. J. Chen, Y. F. Lin, X. H. Gong, Z. D. Luo and Y. D. Huang, *J. Alloys Compd.*, 2009, **484**, 529–534.
- X. Huang and G. Wang, *J. Alloys Compd.*, 2009, **475**, 693–697.
- X. Huang, Z. Hu, Z. Lin and G. Wang, *J. Cryst. Growth*, 2005, **276**, 177–181.
- V. Volkov, C. Cascales, A. Kling and C. Zaldo, *Chem. Mater.*, 2005, **17**, 291–300.
- L. Yi, X. He, L. Zhou, F. Gong, R. Wang and J. Sun, *J. Lumin.*, 2010, **130**, 1113–1117.
- A. V. Zaushitsyn, V. V. Mikhailin, A. Yu. Romanenko, E. G. Khaikina, O. M. Basovich, V. A. Morozov and B. I. Lazoryak, *Inorg. Mater.*, 2005, **41**, 766–770.
- X. Zhou, T. Zhou, Y. Li and Q. Feng, *J. Rare Earths*, 2012, **30**, 315–319.



- 10 J. P. M. Van Vliet and G. Blasse, *J. Solid State Chem.*, 1988, **76**, 160–166.
- 11 Y. Li and X. Liu, *J. Lumin.*, 2014, **151**, 52–56.
- 12 L. Li, J. Zhang, W. Zi, S. Gan, G. Ji, H. Zou and X. Xu, *Solid State Sci.*, 2014, **29**, 58–65.
- 13 G. Benoît, J. Véronique, A. Arnaud and G. Alain, *Solid State Sci.*, 2011, **13**, 460–467.
- 14 Z. Wang, H. Liang, M. Gong and Q. Su, *Mater. Lett.*, 2008, **62**, 619–622.
- 15 Z. Wang, H. Liang, M. Gong and Q. Su, *Opt. Mater.*, 2007, **29**, 896–900.
- 16 Z. Wang, H. Liang, M. Gong and Q. Su, *J. Alloys Compd.*, 2007, **432**, 308–312.
- 17 T. Kimand and S. Kang, *J. Lumin.*, 2007, **122–123**, 964–966.
- 18 E. N. Ipatova, R. F. Klevtsova, L. P. Solov'eva and P. V. Klevtsov, *J. Struct. Chem.*, 1982, **23**, 418–422.
- 19 D. Zhao, J. Zhu, P. Liang, H. Chang and R. He, *Acta Crystallogr., Sect. E: Struct. Rep. Online*, 2012, **68**, i14.
- 20 L. P. Kozeeva and P. V. Klevtsov, *Izv. Acad. Nauk SSSR, Neorg. Mater.*, 1972, **8**, 1328–1329.
- 21 Y. Le Page and P. Strobel, *Acta Crystallogr., Sect. B: Struct. Crystallogr. Cryst. Chem.*, 1980, **36**, 1919–1920.
- 22 M. Moser, D. Klimm, S. Ganschow, A. Kwasniewski and K. Jacobs, *Cryst. Res. Technol.*, 2008, **43**, 350–354.
- 23 Bruker AXS Topas 4.2, 4.2; Karlsruhe, Germany, 2009.
- 24 Program X-Area, X-RED, Stoe&Cie; Darmstadt, Germany, 2009; Program X-SHAPE, Stoe&Cie; Darmstadt, Germany, 2009.
- 25 G. Sheldrick, *Acta Crystallogr., Sect. A: Found. Crystallogr.*, 2008, **64**, 112–122.
- 26 L. Farrugia, *J. Appl. Crystallogr.*, 2012, **45**, 849–854.
- 27 K. Binnemans, *Coord. Chem. Rev.*, 2015, **295**, 1–45.
- 28 X. Y. Chen and G. K. Liu, *J. Solid State Chem.*, 2005, **178**, 419–428.
- 29 C. Ronda, *Luminescence – From Theory to Applications*, Wiley-VCH, Weinheim, 2008.

